



In situ measurement of the stiffness increase in the posterior sclera after UV-riboflavin crosslinking by optical coherence elastography

MARIA VINAS-PENA, *  XU FENG,  GUO-YANG LI, AND SEOK-HYUN YUN

Wellman Center for Photomedicine and Harvard Medical School, Massachusetts General Hospital, 50 Blossom St., Boston, MA, USA

*mvinaspena@mgh.harvard.edu

Abstract: Scleral crosslinking may provide a way to prevent or treat myopia by stiffening scleral tissues. The ability to measure the stiffness of scleral tissues *in situ* pre and post scleral crosslinking would be useful but has not been established. Here, we tested the feasibility of optical coherence elastography (OCE) to measure shear modulus of scleral tissues and evaluate the impact of crosslinking on different posterior scleral regions using *ex vivo* porcine eyes as a model. From measured elastic wave speeds at 6 - 16 kHz, we obtained out-of-plane shear modulus value of 0.71 ± 0.12 MPa ($n = 20$) for normal porcine scleral tissues. After riboflavin-assisted UV crosslinking, the shear modulus increased to 1.50 ± 0.39 MPa ($n = 20$). This 2-fold change was consistent with the increase of static Young's modulus from 5.5 ± 1.1 MPa to 9.3 ± 1.9 MPa after crosslinking, which we measured using conventional uniaxial extensometry on tissue stripes. OCE revealed regional stiffness differences across the temporal, nasal, and deeper posterior sclera. Our results show the potential of OCE as a noninvasive tool to evaluate the effect of scleral crosslinking.

© 2022 Optica Publishing Group under the terms of the [Optica Open Access Publishing Agreement](#)

1. Introduction

Prevalence of myopia have rapidly increased worldwide in the last few decades. It now affects 25-30% of the population in western countries and over 80-90% of the young population in many countries in Asia [1,2]. Myopia is intimately related to the excessive eye growth in the axial direction, which results in blurred retinal images and poor vision. Currently, refractive correction remains the only option to compensate for the blurred images in mild and moderate myopia. In advanced or pathologic myopia, however, serious optical distortion hinders effective vision correction. Furthermore, high myopia is a risk factor in other serious vision-threatening diseases, such as retinal detachment and glaucoma [3].

A variety of interventions has been investigated to manage myopia progression. Multifocal contact lenses [4] have shown some effect in slowing down the progression of myopia by providing the patients with adequate visual and physiological signals that could normalize the eye growth [5,6]. Considerable efforts have been devoted to the development of pharmaceutical approaches that target the eye growth. In recent clinical trials, low-dose atropine eye drops showed the effect of retarding myopia progression in children [7]. While promising, however, much remains to be understood and optimized for this and other drugs to become clinically established [8].

The sclera plays an important role in ocular growth [9]. Strong phenomenological correlations have been found between myopia and the microstructure of scleral tissues [10]. The sclera covers the entire eyeball except for the cornea, and its typical thickness increases from about 0.5 mm in the anterior to ~1.3 mm in the posterior regions [11]. It is composed of collagen fibrils arranged in irregular and interlacing bundles [12] with regional differences. The specific arrangement is responsible for the stiffness of the eyeball. Examination of scleral tissues in myopic eyes showed

smaller scleral thickness associated with a decreased collagen fibril diameter and a narrowing of collagen fiber bundles [13] and enhanced enzymatic degradation of the extracellular matrices [14], as well as the loss of scleral tissue integrity, mechanical weakening, and regional differences [15,16]. Advanced myopia develop posterior staphyloma [10,17].

Based on all the evidence, a procedure known as scleral collagen crosslinking (SCXL) has been suggested. SCXL aims at stiffening the posterior sclera to retard the axial length growth of the eye and is built on the clinical success of corneal crosslinking (CXL) [18] that is used to treat corneal ectatic disorders. The methods for crosslinking use light activation of a photosensitizer such as riboflavin by UVA light [19], or rose Bengal by green light [20]. Chemical crosslinking using glycerinaldehyde, genipin, or formaldehyde releasers-FARs has also been explored in preclinical studies [21–23]. Wollensak *et al.* were the first to propose the CXL of the sclera for the prevention of myopic progression [24]. Using riboflavin and UVA, they found a 160% increase in the rigidity of porcine and human sclera *ex vivo* and attributed the change to the formation of inter-fibrillar chemical covalent bonds. Since then, various SCXL methods in animal models of myopia [25–27] have shown efficacy in reducing axial length elongation, primarily targeting equatorial scleral tissues [19,28]. Liu *et al.* showed that SCXL increased the density of the fiber bundles [26], resulting in increased stiffness.

The development of SCXL requires tools to evaluate the effects on crosslinking on the mechanical properties of tissues. Standard mechanical testing, such as extensometry, has been widely used with scleral tissues extracted from the eyes [17]. Inflation tests based on intraocular pressure (IOP) variation has been applied to intact eye globes [29,30], but this technique relies on large IOP modulation above normal physiological ranges. Brillouin light scattering microscopy has allowed to evaluate the longitudinal moduli of the corneal [31] and scleral [32] tissues *in vivo*. Optical coherence elastography (OCE) has emerged as a promising technique with high spatial resolution and high sensitivity [33–35]. Air-puff-based OCE technique [36,37] allowed the reconstruction of corneal [38] and scleral [39] mechanical properties via finite element modeling (FEM) [30,40]. The stiffness of the sclera affects the magnitude of corneal deformation against air-puffs [41]. Bronte-Ciriza *et al.* used this technique to evaluate the sclera of *ex vivo* porcine eyes [39] and estimated the scleral Young's modulus to be 1.84 ± 0.30 MPa in the equatorial inferior region and 6.04 ± 2.11 MPa in the equatorial temporal region. Wave-propagation-based OCE has been applied to the anterior scleral region for the measurement of the shear modulus *ex vivo* [42] and *in vivo* [43]. Ramier *et al.* used a miniature contact probe [44] to excite low-energy elastic waves at high frequencies (up to 16 kHz) and demonstrated high-resolution measurement of shear modulus in the cornea and anterior sclera in 12 healthy subjects [43]. Compared to the cornea, the mechanical properties of the sclera are more spatially heterogeneous, anisotropic, and varying locally and from the anterior to posterior regions.

Here, we apply the high-frequency OCE technique to measure the heterogeneous mechanical properties of posterior scleral tissues and, for the first time to our knowledge, evaluate the changes in shear moduli after SCXL. As a model system, we use *ex vivo* in porcine eyes and riboflavin-assisted UV crosslinking. The measurement is compared with uniaxial tensile tests of strips. We discuss the potential of OCE as a tool to evaluate the biomechanical effect of SCXL in human patients.

2. Methods

2.1. OCE system

Our OCE system has been built based on a custom-built, swept-source optical coherence tomography (OCT) system previously described [43,45]. It uses a home-built, polygon-swept laser source (center wavelength: 1300 nm, bandwidth: 108 nm, A-line rate 43.2 kHz). The sample arm consists of a 2-axis galvanometer scanner and an objective lens (working distance:

64 mm, transverse resolution: 30 μm). The axial and transverse resolution of the OCT system are $\sim 15 \mu\text{m}$ and $\sim 30 \mu\text{m}$ in air.

The excitation of Lamb waves was achieved by using a home-built piezoelectric probe, which consists of a 3D printed probe tip (2 mm diameter) glued on a piezoelectric transducer (PZT) [44]. The probe is mounted on a translation stage and brought to physical contact with the eye sample (Fig. 1(a)). A multi-purpose input/output board (USB-6353, National Instruments) was used to generate analog waveforms to operate the galvanometer scanner and the mechanical probe. The waveforms were synchronized to the optical clock of fiber Bragg grating, ensuring phase-synchronous operation. In this experiment, the frequency of vibration was step-tuned from 6 to 16 kHz with an interval of 2 kHz with a duration of ~ 4 ms (172 A-lines per B-scan) at each frequency, and the frequency ramp was repeated up to 10 times (10 s) while the OCT beam was scanned along the horizontal axis from the contact tip. The measured peak wave amplitude was ~ 100 nm at 6 kHz and ~ 20 nm at 16 kHz at the tissue surface. The beam-scan length decreases with the frequency from 10 mm at 6 kHz to 4 mm at 16 kHz, allowing 96 spatial points to be acquired at each frequency. A complete OCE scan at a specific tissue location took approximately 2.3 s.

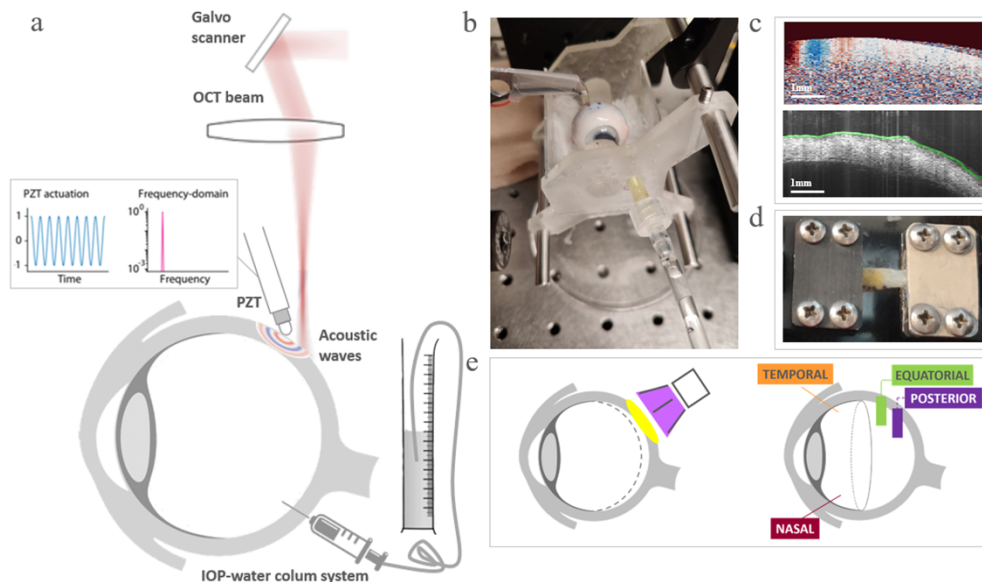


Fig. 1. Experimental overview. (a) OCE setup with a swept-source OCT system, humidity chamber, and water column. (b) Contact probe and measurement setup. (c) Example of vibrography and intensity images of a treated eye. (d) Tensile test setup. (e) Illustration of the crosslinking procedure and different anatomical locations. Color bars (green and purple) illustrate the location and length of the region of interest, from the inferior to superior locations, for OCE measurements and tensile tests.

2.2. Experimental set-up and protocol

20 porcine eyes (10 pairs) were obtained from a local slaughterhouse, and all measurements were performed within 24 hours postmortem. The connective tissues, such as fat, muscles, and the optic nerve, were removed. A customized wet chamber was built to hold an eye globe and avoid dehydration during measurements and treatments (Fig. 1(b)). The eye was placed over cotton soaked in PBS solution to maintain the humidity, immobilized, and connected to an IOP controlling water column by a needle to maintain a constant IOP at 15 mmHg. For each

eye sample, a complete set of measurements including OCE, and uniaxial tensile testing were performed. First, OCE measurements were performed in the whole eyes before treatment, after instillation of riboflavin, and after treatment, respectively. After the measurements, strips were cut following same direction that the OCE regions (treated area and contralateral non treated area) and uniaxial tensile tests were performed. An additional control measurement was performed on contralateral, untreated tissues extracted from the eye globe. The entire measurement took about 3.5 hours per eye.

2.2.1. OCE measurement

A porcine eye in the humidity chamber was aligned with the OCT beam, and the PZT probe was brought to the contact with the sclera. The probe was gently pressed perpendicularly on to the tissue. After the probe tip has made a contact with the sclera, it was gently advanced by ~ 100 μm further to ensure stable mechanical contact to be maintained during stimulus actuation. The small deformation of the tissue by the static pressure of the probe does not affect the wave speed and IOP, as confirmed by repeated OCE measurements with different stress levels of the probe. For repeatability, two separate OCE measurements were performed in adjacent locations in the same region, each time retracting the probe tip from the eye and repositioning it to the tissue. No apparent near-field evanescent waves were observed. Two different posterior scleral regions were targeted: posterior sclera about 3 mm behind the equatorial region of the eye, which we referred to as “EQUATORIAL”, and posterior sclera about 6 mm behind the equator and around the optical nerve region, referred to as “POSTERIOR”. The lateral extent of each region was 3 mm. For each the equatorial or posterior region, scleral tissues in the nasal (N) and temporal (T) regions were separately investigated. The measurements were performed before treatment, after 30-min soaking with riboflavin, and after SCXL.

2.2.2. SCXL procedure

Riboflavin-UVA light cross-linking (UVX-SCXL) [46,47] treatment was applied to a 10-mm-diameter-region in each eye. Riboflavin solution consisted of 0.1% riboflavin-5-phosphate in 20% Dextran (D5376-100G Dextran from leuconostoc mesenteroides, Sigma Life Science). Treatment was applied using a commercial device (Avedro, Inc. KXL® System, Glaukos) equipped with a 370 nm light source [48]. The UVX-SCXL protocol involves 30-min staining by soaking with riboflavin solution, during which a drop of riboflavin solution is applied every 5 min, followed by UVA irradiation for 30 min with 3 mW/cm^2 with one drop of riboflavin applied every 5 min. SCXL was applied in one posterior scleral region per eye.

2.2.3. Tensile test

Scleral strips (each 4 mm by 20 mm) were cut from both treated (2 strips) and contralateral control (2 strips) regions, along the wave propagation direction from the inferior to superior regions, for measurement in a uniaxial stretcher. A 10-N horizontal load cell with a MTest-Quattro controller (Micro EP Miniature; Admet) was used to perform 6-N load, 3 cycle measurement. The loading and unloading time of each cycle was kept low to ensure low strain rates (jog rate: 2 mm/min; home rate: 10 mm/min). The axial stress on the strip was determined by the recorded force divided by the actual cross-sectional area (the width times the thickness) of the scleral strip at different strain levels. The scleral strip was anchored in serrated clamps separated by 5 mm to set initial specimen length and preloaded to 0.05 N tension to eliminate slack.

2.3. Data analysis

To derive shear modulus from the OCE data, the wave speed for each stimulus frequency was obtained by measuring the wavelength of the elastic wave [44]. Since elastic waves are guided by the scleral tissues with finite thickness, the dispersion relationship of the guided elastic waves

(the wave speed as a function of the frequency) was fit using the Lamb acoustic wave model [44], and the out-of-plane shear modulus determined. The tissue thickness was obtained from the OCT structural images using edge detection, and the average value near the beginning of the wave profiles, where the amplitude is the highest, was used for curve fitting. The sclera was modeled as a thin, incompressible elastic layer with a density of 1000 kg/m^3 , supported by a semi-infinite fluid (aqueous humor). The outside of the sclera was assumed to be free space imposing the stress-free boundary condition. The dispersion relation of this model has been well studied [49,50]. We used least-square regression fitting to the wave dispersion using scleral shear modulus as the only fitting parameter in the range of 6 to 16 kHz. While the sclera is modeled as an elastic layer, the apparent amplitude decay suggests the viscoelastic properties. To characterize the viscosity, we also measured the $1/e$ propagation distance by determining the amplitude attenuation [44].

From the stress-strain curves in the extensometry measurement, the in-plane Young's modulus value was calculated at 1%, 5% and 10% strain levels, respectively. The percentage change of elastic modulus was calculated as $(A - B)/B \times 100\%$, where B and A represents the measured values before and after SCXL, respectively. For example, a 100% increase means a 2-fold increase. Statistical analysis was performed with SPSS Statistics software (IBM) to test statistically significant differences between conditions (paired-samples t-test across conditions).

3. Results

3.1. Regional variation of shear & Young's moduli of intact porcine eyes

Figure 2(a) shows the thickness variation in the temporal and nasal regions which we measured from the OCT images of the impact point of the tip on the porcine eyes ($n = 20$). The measured thickness in the posterior locations was higher than the equatorial region in both temporal and nasal regions by 20% (EQUATORIAL: $0.89 \pm 0.03 \text{ mm T}$ & $0.81 \pm 0.02 \text{ mm N}$ & $0.85 \pm 0.02 \text{ mm All}$; POSTERIOR: $1.06 \pm 0.04 \text{ mm T}$ & $0.97 \pm 0.04 \text{ mm N}$ & $1.01 \pm 0.04 \text{ mm All}$). A similar trend has been reported for the human sclera [11,17].

Figure 2(b) shows the average wave speeds distribution measured at different frequencies (6-16 kHz) in the EQUATORIAL location for all 20 eyes. The high-frequency (16 kHz) limit provided a good estimate of the scleral Rayleigh-wave velocity, v_R , (EQUATORIAL $19.8 \pm 2.3 \text{ m/s}$ & POSTERIOR $21.6 \pm 2.5 \text{ m/s}$). These values are similar to those obtained in the previous *in vivo* OCE measurements of the human sclera [43].

Figure 2(c) shows the $1/e$ propagation distance of the elastic waves in the 20 eyes. On average, the propagation distance was higher in the posterior region compared to the equatorial location (EQUATORIAL $2.60 \pm 0.28 \text{ m}$ at 6 kHz; $1.24 \pm 0.14 \text{ m}$ at 16 kHz & POSTERIOR $2.90 \pm 0.27 \text{ m}$ at 6 kHz; $1.35 \pm 0.15 \text{ m}$ at 16 kHz). The mean elastic wave speed for each posterior sclera location differed statistically significantly for the different locations (Fig. 2(d-f)). The wave speed in the posterior region, averaged across frequencies, was slightly higher than the equatorial region in both temporal and nasal positions by about 13% (POSTERIOR $19.52 \pm 0.76 \text{ m/s}$, EQUATORIAL $17.23 \pm 0.78 \text{ m/s}$; TEMPORAL POSTERIOR $20.88 \pm 0.80 \text{ m/s}$, EQUATORIAL $18.94 \pm 0.80 \text{ m/s}$, NASAL POSTERIOR $18.16 \pm 0.75 \text{ m/s}$, and EQUATORIAL $15.5 \pm 0.78 \text{ m/s}$). We note that the wave speed was sensitive to the IOP with a linear coefficient of $\sim 10\%$ increase every 5 mmHg in the range of 5 to 20 mmHg. (In a trial experiment using an eye globe, we measured wave speeds of 17–20 m/s at 5 mmHg, 15–22 m/s at 7.5 mmHg, 17–25 m/s at 10 mmHg, and 18–27 m/s at 15 mmHg). In all the experiments, we maintained the IOP at 15 mmHg.

Figure 3 shows the shear modulus obtained from the fitting of the wave speed elastography data (6-16 kHz) in all measured eyes for different regions. The average shear modulus in the posterior region was $0.71 \pm 0.12 \text{ MPa}$ whereas that in the equatorial region was $0.58 \pm 0.14 \text{ MPa}$. This is compared to 0.51 MPa previously measured in the human anterior sclera using the same OCE system [43]. The regional difference is apparent in both temporal and nasal sides.

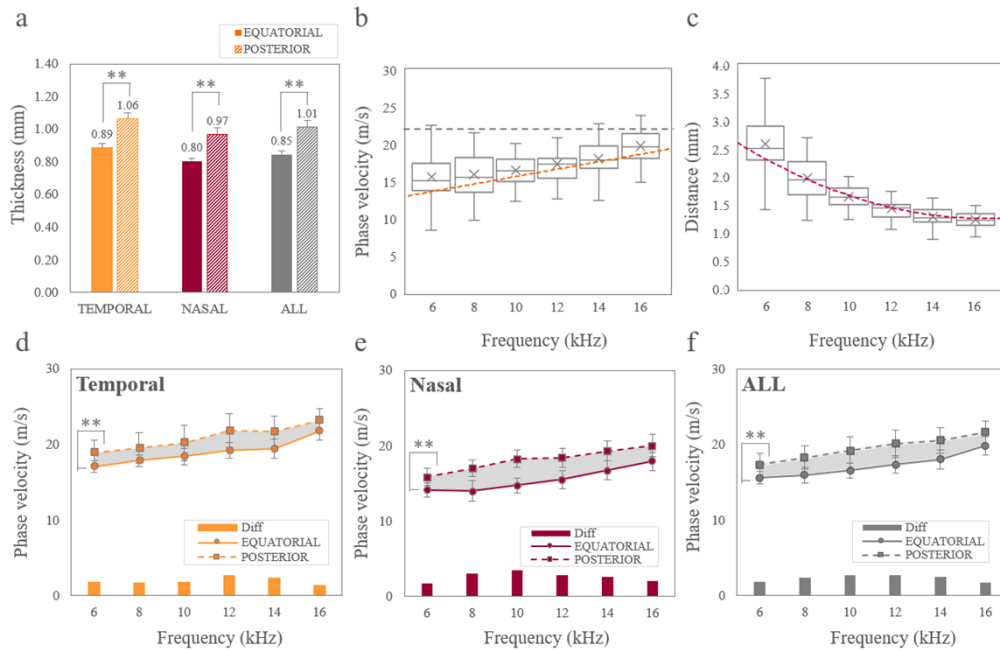


Fig. 2. Posterior sclera mechanical properties regional variation. a) Averaged local scleral thickness measured from OCT intensity images. Error bars shows inter sample variation. (b) Averaged wave speeds for all 20 eyes measured at posterior equator sclera (EQUATORIAL) as a function of frequency (6-16 kHz). Dashed line (black): speed high-frequency limit (Rayleigh surface wave speed). Dashed line (orange): curve fit. (c) The averaged $1/e$ propagation distance for EQUATORIAL region. Dashed line (magenta): curve fit. (d) Averaged phase velocity for EQUATORIAL (solid line) and POSTERIOR (dashed line) for all 10 eyes in the temporal location. (e) Averaged phase velocity for EQUATORIAL (solid line) and POSTERIOR (dashed line) for all 10 eyes in the nasal location. (f) Averaged phase velocity for EQUATORIAL (solid line) and POSTERIOR (dashed line) for all 20 eyes in the temporal location. Solid bars in (d-f) stand for the difference between locations at each frequency. *, $p < 0.05$. **, $p < 0.01$.

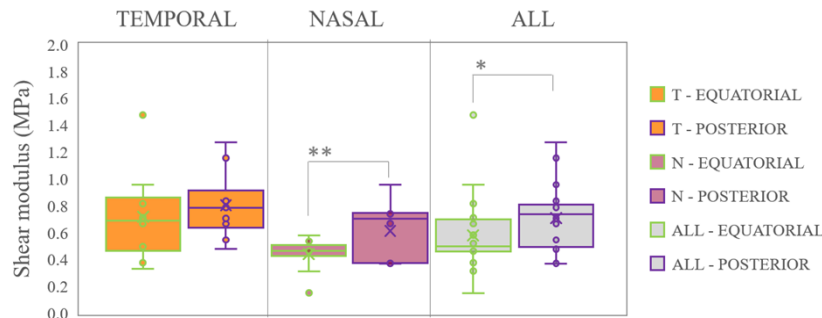


Fig. 3. Shear modulus. Out-of-plane shear modulus, G , obtained from OCE measurements in EQUATORIAL (green) and POSTERIOR (purple) locations for all eyes. *, $p < 0.05$. **, $p < 0.01$.

Following the OCE measurements, we removed scleral tissue strips from the eye globes and performed standard tensile testing. Figure 4 shows the in-plane Young's modulus values obtained from stress-strain curves at 5% and 10% strain levels, respectively. 5%-strain tensile Young's modulus was not statistically different between different regions. However, 10%-strain Young's modulus was higher in the posterior region (3.70 ± 0.9 MPa) compared to the equatorial region (3.02 ± 0.7 MPa) by about 35%. For comparison, Elsheikh *et al.* have previously measured the uniaxial tensile modulus of the human sclera and reported 30-40 kPa at a 1% strain level [17].

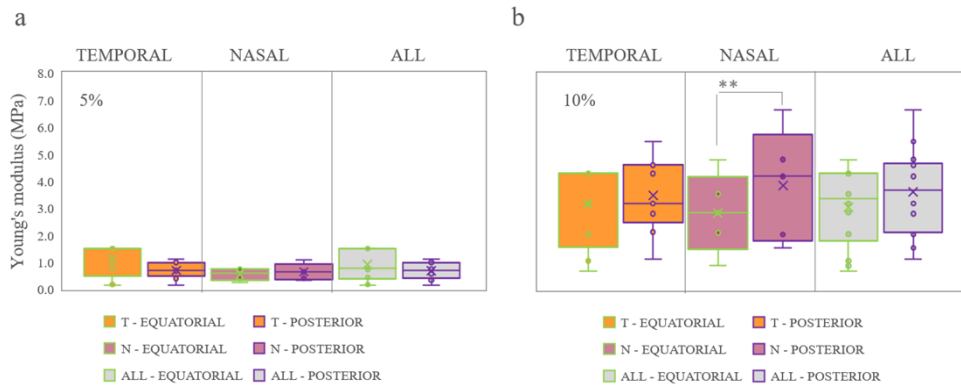


Fig. 4. Young's modulus. Young's modulus measured from tensile tests at 5% strain, (a), and 10% strain, (b). The test tissue samples were dissected from 4 different locations of the eye globes. **, $p < 0.01$.

3.2. Impact of scleral crosslinking on the posterior sclera mechanical properties

We first checked the effect of riboflavin alone on the tissue properties. Figure 5 (a-b) shows the elastic wave speeds and thickness change after 30-min soaking with riboflavin solution without UV irradiation, compared to controls. The 30-minute riboflavin soaking produced about 10% increase of the phase speed in the equatorial region and about 3% decrease in the posterior region. The soaking increased the thickness by about 1% in both regions.

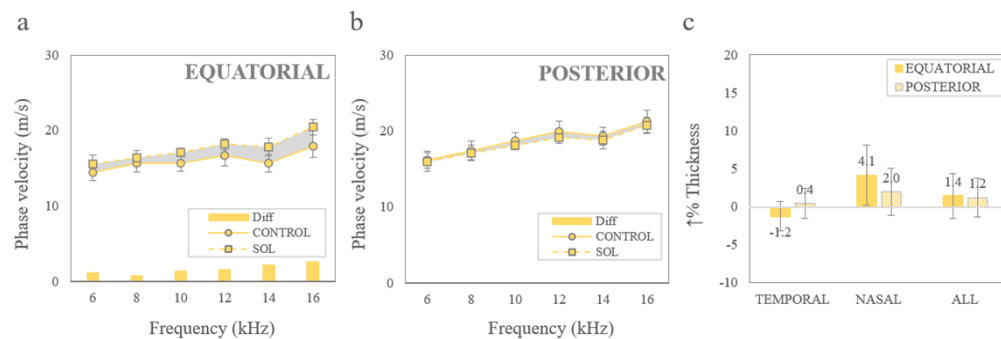


Fig. 5. Impact of riboflavin soaking on the posterior sclera mechanical properties.

Averaged phase velocity for control (solid lines) and after soaking conditions (sol, dashed lines) for EQUATORIAL, (a), and POSTERIOR, (b), locations for all 20 eyes. Solid yellow bars stand for the difference between locations at each frequency; (c) Increase of thickness after riboflavin soaking. Error bars stand for inter-subject variation.

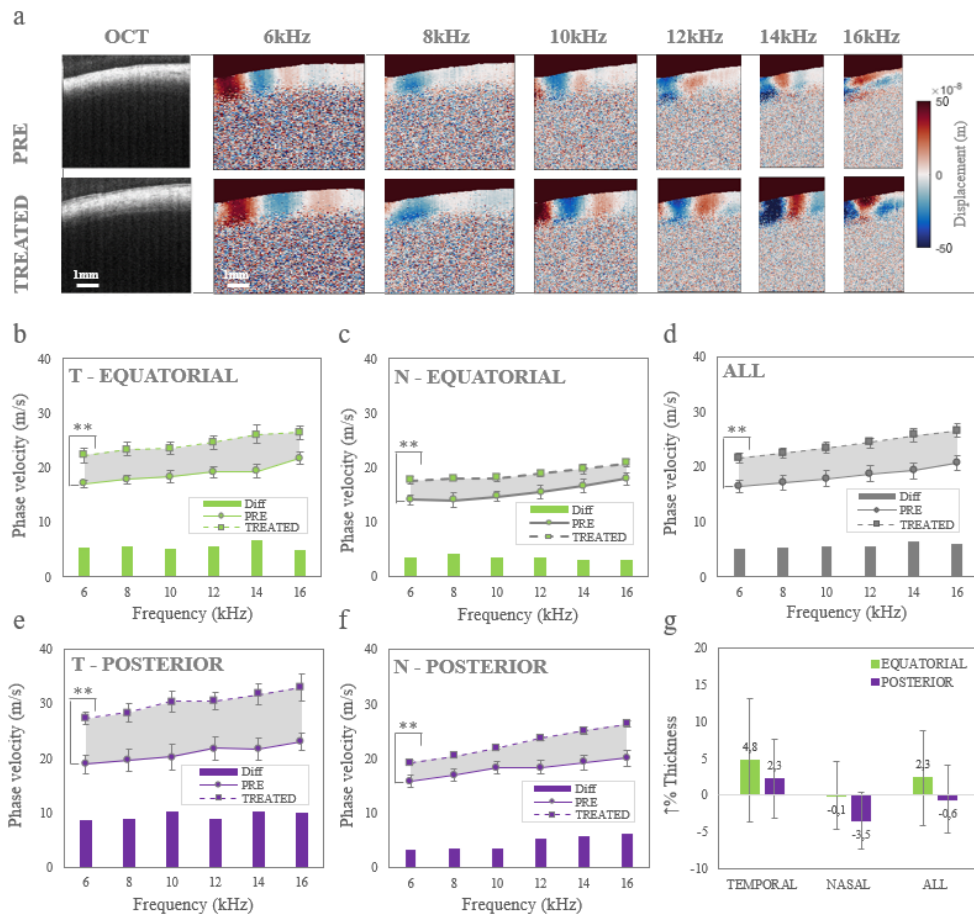


Fig. 6. Wave speed and thickness change after crosslinking treatment. (a) Intensity and vibrography series of images obtained before (PRE) and after the treatment (TREATED) for frequencies ranging from 6 - 16 kHz. Averaged phase velocity for pre (solid lines) and after treatment conditions (dashed lines) for T-EQUATORIAL (b) and N-EQUATORIAL (c), T-POSTERIOR (e) and N-POSTERIOR (f), and (d) averaged across all conditions. (g) Increase of thickness (%) after treatment in EQUATORIAL (green bars) and POSTERIOR (purple bars) locations. Error bars stand for inter-subject variation. *, $p < 0.05$. **, $p < 0.01$.

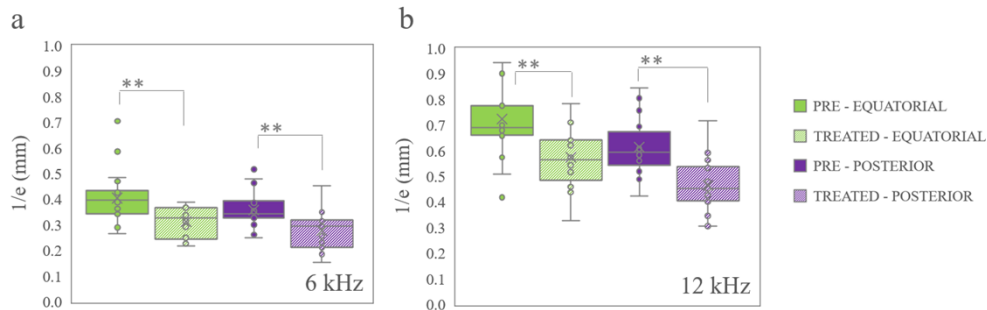


Fig. 7. Propagation distance. The $1/e$ propagation distance of the elastic waves in the sclera at 6 kHz, (a), and 12 kHz, (b). *, $p < 0.05$. **, $p < 0.01$.

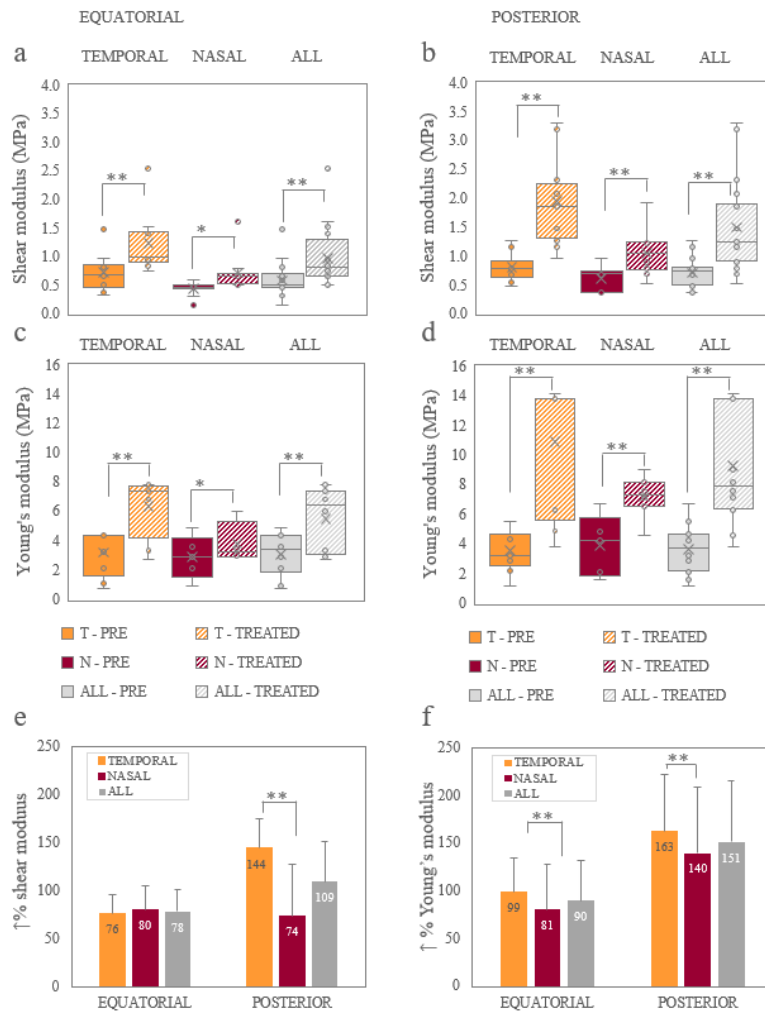


Fig. 8. Shear & Young's modulus of the posterior sclera after SCXL. Shear modulus obtained from the wave speed data for EQUATORIAL (a) and POSTERIOR (b) locations before (solid bars) and after SCXL (dashed bars). Young's modulus obtained from the tensile test data for EQUATORIAL (c) and POSTERIOR (d) locations before (solid bars) and after SCXL (dashed bars). The amount of increase in % (100% means a 2-fold increase) of the shear modulus (e) and the Young's modulus (f) after SCXL. *, $p < 0.05$. **, $p < 0.01$.

Next, we measured the effects of SCXL. Figure 6 (a) shows an example of the intensity and vibrography series of images obtained before and after the treatment for frequencies ranging from 6 - 16 kHz, while Fig. 6 (b-f) shows the wave speed differences between before and after treatment at different regions. The wave speed increased significantly after treatment across all conditions by 31% on average. Some regional dependence in the change was observed. The temporal, posterior region showed the most increase in the wave speed by 45%. Despite these significant changes, no statistically significant change in the scleral thickness was observed (Fig. 6(g)). Additional control measurements, performed in a contralateral position of the treated area, showed no changes in the mechanical properties out of the treated area.

The elastic waves are attenuated by viscous damping in the tissue. We analyzed the propagation distance ($1/e$) of the waves. Figure 7 shows the propagation distance measured at 6 kHz and 12

kHz, respectively, at four different locations in the eye globe. After treatment, the propagation distance was decreased significantly at both frequencies.

Figure 8 shows a summary of the SCXL-induced changes in out-of-plane shear modulus at 6-12 kHz and in-plane quasi-static Young's moduli. Shear modulus increased significantly after treatment, from 0.58 ± 0.14 MPa to 0.97 ± 0.25 MPa in the equatorial region and from 0.71 ± 0.12 MPa to 1.50 ± 0.38 MPa ($p < 0.05$) in the posterior region. Similarly, Young's modulus increased significantly after treatment by 2 to 2.5 folds. Overall, the treatment made significantly larger changes in the temporal than nasal regions.

4. Discussion

In this study we have used, for the first time to our knowledge, OCE to evaluate the changes in the mechanical properties of posterior scleral tissues after crosslinking of *ex vivo* porcine eyes. The OCE enabled us to determine out-of-plane shear modulus at kHz range. Using porcine eyes *ex vivo* at 15 mmHg, we measured baseline shear modulus values of 0.71 ± 0.12 MPa in the posterior sclera and 0.58 ± 0.14 MPa in the equatorial sclera. These values are comparable to 0.30 to 0.51 MPa we have measured in the human anterior sclera *in vivo* by using the same OCE system [43]. The baseline Young's modulus values measured by standard tensile tests were also similar to previous measurements [39]. The wave speed was changed by $\sim 10\%$ for every 5 mmHg change of the IOP, in agreement with previous results [42,51,52]. After SCXL, the shear moduli of the sclera increased to 1.50 ± 0.39 MPa on average. Changes of shear modulus were significantly higher in the temporal than nasal regions, which is consistent with previous observations in the scleral stiffness [53] and microstructure [54]. The magnitude of change was higher in the temporal than nasal regions of the posterior sclera. The 2-fold change is slightly smaller than that obtained by Wollensak *et al.* using riboflavin (160%) in porcine eyes and by Villegas *et al.* using riboflavin (230%) and rose bengal (380%) in rabbit eyes, all measured by extensometry. The differences in the % changes are reasonable, considering the differences in the experimental conditions and measurement techniques.

The scleral tissues have anisotropic microstructure with laterally arranged collagen fibers [55]. Our measured values of out-of-plane shear modulus were about 5-6 times lower than those of in-plane Young's modulus. Although direct comparison needs care because of the difference in the time scale of the measurement, the large difference is reasonable considering the mechanical anisotropy between in and out of plane. To minimize compounding effects due to transverse anisotropy and regional heterogeneity, we have always measured waves propagating from the inferior to posterior region, where the thickness of scleral tissue was relatively uniform with a standard deviation less than $40 \mu\text{m}$ ($< 5\%$ of thickness). In our tissue model, the guided wave speed is primarily governed by out-of-plane shear modulus, whereas the tensile stiffness is governed by the in-plane tensile modulus. The effect of in-plane shear or tensile modulus to the wave speed is negligible compared with the standard deviations of our measurements [56,57]. Despite the fact that the two moduli are two independent parameters and were measured at different frequencies (~ 10 kHz versus quasi-static), our experiments suggest both mechanical moduli have significantly been increased by about 2-fold after SCXL. This consistent increase indicates that it is not essential to measure anisotropy to characterize crosslinking, and the OCE measurement can be used to monitor scleral crosslinking *in situ*, instead of invasive mechanical tests.

Interestingly, the propagation distance after treatment decreased more than the decrease of the wave wavelength. This result may indicate increased viscosity of tissue after SCXL. Accurate characterization of a tissue's material properties can lead to a broader understanding of the mechanisms that underlie tissue damage, as well as determine the resultant altered load-bearing behavior of a remodeled or healed tissue. For example, changes in the viscoelastic material properties of monkey peripapillary sclera have been proposed for earliest detectable stage of

glaucomatous damage [58], indicating damaged and/or remodeled extracellular matrix (ECM) of the tissue. Cellular mechanotransduction and ECM remodeling have been reported in other load-bearing collagenous tissues, in which fibroblasts secrete factors that elicit changes in the surrounding ECM in response to an increase in strain [59]. It is likely that such strain-induced changes in protein and genetic factor expression act to increase the resistance of the ECM to further strain. Understanding the changes behind SCXL will allow to improve the technique and increase the possibility of *in vivo* studies.

Our data suggest that OCE provide appropriate spatial resolution and sensitivity to quantify the mechanical moduli of scleral tissues. The ability to measure the local changes of scleral mechanical properties noninvasively before and after SCXL is expected to be useful for optimizing the procedure and for assessing the treatment effect. With appropriate fiber-optic catheters [60], OCE holds the promise to be a useful tool to evaluate the biomechanical changes in posterior sclera following crosslinking treatments in myopic eyes of patients.

Funding. National Institutes of Health (R01-EB027653 and R42-EY028820 to SY); HORIZON EUROPE Marie Skłodowska-Curie Actions (H2020-MSCA-IF-GF-2019-MYOMICRO-893557 to MV).

Acknowledgement. The authors thank Prof. Irene Kochevar for giving access to the Avedro device for SCXL, and Prof. Robert Redmond and Nicholas King for the tensile test device.

Disclosures. The authors declare no conflicts of interest.

Data Availability. Data underlying the results presented in this paper are not publicly available at this time but may be obtained from the authors upon reasonable request.

Supplemental document. See [Supplement 1](#) for supporting content.

References

1. B. A. Holden, T. R. Fricke, D. A. Wilson, M. Jong, K. S. Naidoo, P. Sankaridurg, T. Y. Wong, T. J. Naduvilath, and S. Resnikoff, "Global prevalence of myopia and high myopia and temporal trends from 2000 through 2050," *Ophthalmology* **123**(5), 1036–1042 (2016).
2. E. Dolgin, "The myopia boom," *Nature* **519**(7543), 276–278 (2015).
3. D. I. Flitcroft, "The complex interactions of retinal, optical and environmental factors in myopia aetiology," *Prog. Retinal Eye Res.* **31**(6), 622–660 (2012).
4. S. Vedhkrishnan, M. Vinas, C. Benedi-Garcia, P. Casado, and S. Marcos, "Visual performance with multifocal lenses in young adults and presbyopes," *PLoS One* **17**(3), e0263659 (2022).
5. S. Vedhkrishnan, M. Vinas, S. Aissati, and S. Marcos, "Vision with spatial light modulator simulating multifocal contact lenses in an adaptive optics system," *Biomed. Opt. Express* **12**(5), 2859–2872 (2021).
6. M. Vinas, S. Aissati, A. M. Gonzalez-Ramos, M. Romero, L. Sawides, V. Akondi, E. Gamba, C. Dorronsoro, T. Karkkainen, D. Nankivil, and S. Marcos, "Optical and visual quality with physical and visually simulated presbyopic multifocal contact lenses," *Trans. Vis. Sci. Tech.* **9**(10), 20 (2020).
7. P. C. Wu, M. N. Chuang, J. Choi, H. Chen, G. Wu, K. Ohno-Matsui, J. B. Jonas, and C. M. G. Cheung, "Update in myopia and treatment strategy of atropine use in myopia control," *Eye* **33**(1), 3–13 (2019).
8. J. J. Walline, K. B. Lindsley, S. S. Vedula, S. A. Cotter, D. O. Mutti, S. M. Ng, and J. D. Twelker, "Interventions to slow progression of myopia in children," *Cochrane Database Syst. Rev.* **1**(1), CD004916 (2011).
9. R. Metlapally and C. F. Wildsoet, "Scleral mechanisms underlying ocular growth and myopia," *Prog. Mol. Biol. Transl. Sci.* **134**, 241–248 (2015).
10. J. A. Rada, S. Shelton, and T. T. Norton, "The sclera and myopia," *Exp. Eye Res.* **82**(2), 185–200 (2006).
11. C. Boote, I. A. Sigal, R. Grytz, Y. Hua, T. D. Nguyen, and M. J. A. Girard, "Scleral structure and biomechanics," *Prog. Retinal Eye Res.* **74**, 100773 (2020).
12. Y. Komai and T. Ushiki, "The three-dimensional organization of collagen fibrils in the human cornea and sclera," *Invest Ophthalmol Vis Sci* **32**(8), 2244–2258 (1991).
13. B. J. Curtin, T. Iwamoto, and D. P. Renaldo, "Normal and staphylomatous sclera of high myopia. An electron microscopic study," *Arch. Ophthalmol. (Chicago, IL, U. S.)* **97**(5), 912–915 (1979).
14. N. A. McBrien and A. Gentle, "Role of the sclera in the development and pathological complications of myopia," *Prog. Retinal Eye Res.* **22**(3), 307–338 (2003).
15. A. Consejo and J. J. Rozema, "In vivo anterior scleral morphometry, axial length and myopia," *Cont. Lens. Anterior Eye.* **43**(1), 21–25 (2020).
16. F. Zvietcovich and K. V. Larin, "Wave-based optical coherence elastography: The 10-year perspective," *Prog Biomed Eng (Bristol)* **4**(2022).
17. A. Elsheikh, B. Geraghty, D. Alhasso, J. Knappett, M. Campanelli, and P. Rama, "Regional variation in the biomechanical properties of the human sclera," *Exp. Eye Res.* **90**(5), 624–633 (2010).

18. G. Wollensak, E. Spoerl, and T. Seiler, "Riboflavin/ultraviolet-a-induced collagen crosslinking for the treatment of keratoconus," *Am. J. Ophthalmol.* **135**(5), 620–627 (2003).
19. C. Schuldt, A. Karl, N. Korber, C. Koch, Q. Liu, A. W. Fritsch, A. Reichenbach, P. Wiedemann, J. A. Kas, M. Francke, and H. P. Iseli, "Dose-dependent collagen cross-linking of rabbit scleral tissue by blue light and riboflavin treatment probed by dynamic shear rheology," *Acta Ophthalmol.* **93**(5), e328–e336 (2015).
20. D. Cherfan, E. E. Verter, S. Melki, T. E. Gisel, F. J. Doyle Jr., G. Scarcelli, S. H. Yun, R. W. Redmond, and I. E. Kochevar, "Collagen cross-linking using rose bengal and green light to increase corneal stiffness," *Invest. Ophthalmol. Visual Sci.* **54**(5), 3426–3433 (2013).
21. Y. Chu, Z. Cheng, J. Liu, Y. Wang, H. Guo, and Q. Han, "The effects of scleral collagen cross-linking using glyceraldehyde on the progression of form-deprived myopia in guinea pigs," *J. Ophthalmol.* **2016**, 1–8 (2016).
22. M. Wang and C. C. Corpuz, "Effects of scleral cross-linking using genipin on the process of form-deprivation myopia in the guinea pig: a randomized controlled experimental study," *BMC Ophthalmol.* **15**(1), 89 (2015).
23. M. El Hamdaoui, A. M. Levy, M. Gaonkar, T. J. Gawne, C. A. Girkin, B. C. Samuels, and R. Grytz, "Effect of scleral crosslinking using multiple doses of genipin on experimental progressive myopia in tree shrews," *Trans. Vis. Sci. Tech.* **10**(5), 1 (2021).
24. G. Wollensak and E. Spoerl, "Collagen crosslinking of human and porcine sclera," *J. Cataract Refractive Surg.* **30**(3), 689–695 (2004).
25. A. Dotan, I. Kremer, T. Livnat, A. Zigler, D. Weinberger, and D. Bourla, "Scleral cross-linking using riboflavin and ultraviolet-a radiation for prevention of progressive myopia in a rabbit model," *Exp. Eye Res.* **127**, 190–195 (2014).
26. S. Liu, S. Li, B. Wang, X. Lin, Y. Wu, H. Liu, X. Qu, J. Dai, X. Zhou, and H. Zhou, "Scleral cross-linking using riboflavin UVA irradiation for the prevention of myopia progression in a guinea pig model: blocked axial extension and altered scleral microstructure," *PLoS One* **11**(11), e0165792 (2016).
27. S. A. McFadden, M. Coassin, M. S. Mattson, M. H. Howlett, J. A. Kornfield, and D. M. Schwartz, "Scleral strengthening inhibits ocular elongation and induces an alternative response to form deprivation myopia," *Invest. Ophthalmol. Vis. Sci.* **51**, 1192 (2010).
28. M. Wang, F. Zhang, K. Liu, and X. Zhao, "Safety evaluation of rabbit eyes on scleral collagen cross-linking by riboflavin and ultraviolet A," *Clin. Experiment. Ophthalmol.* **43**(2), 156–163 (2015).
29. C. Whitford, A. Joda, S. Jones, F. Bao, P. Rama, and A. Elsheikh, "Ex vivo testing of intact eye globes under inflation conditions to determine regional variation of mechanical stiffness," *Eye (Lond)* **3**(1), 21 (2016).
30. S. Kling, N. Bekesi, C. Dorransoro, D. Pascual, and S. Marcos, "Corneal viscoelastic properties from finite-element analysis of in vivo air-puff deformation," *PLoS One* **9**(8), e104904 (2014).
31. G. Scarcelli, R. Pineda, and S. H. Yun, "Brillouin optical microscopy for corneal biomechanics," *Invest. Ophthalmol. Visual Sci.* **53**(1), 185–190 (2012).
32. P. Shao, S. Besner, J. Zhang, G. Scarcelli, and S. H. Yun, "Etalon filters for Brillouin microscopy of highly scattering tissues," *Opt. Express* **24**(19), 22232–22238 (2016).
33. K. V. Larin and D. D. Sampson, "Optical coherence elastography - OCT at work in tissue biomechanics [Invited]," *Biomed. Opt. Express* **8**(2), 1172–1202 (2017).
34. M. A. Kirby, I. Pelivanov, S. Song, L. Ambrozinski, S. J. Yoon, L. Gao, D. Li, T. T. Shen, R. K. Wang, and M. O'Donnell, "Optical coherence elastography in ophthalmology," *J. Biomed. Opt.* **22**(12), 1–28 (2017).
35. X. Feng, G. Y. Li, A. Ramier, A. M. Eltony, and S. H. Yun, "In vivo stiffness measurement of epidermis, dermis, and hypodermis using broadband Rayleigh-wave optical coherence elastography," *Acta Biomater.* **146**, 295–305 (2022).
36. A. Jimenez-Villar, E. Maczynska, A. Cichanski, M. Wojtkowski, B. J. Kaluzny, and I. Grulkowski, "High-speed OCT-based ocular biometer combined with an air-puff system for determination of induced retraction-free eye dynamics," *Biomed. Opt. Express* **10**(7), 3663–3680 (2019).
37. D. Alonso-Caneiro, K. Karnowski, B. J. Kaluzny, A. Kowalczyk, and M. Wojtkowski, "Assessment of corneal dynamics with high-speed swept source optical coherence tomography combined with an air puff system," *Opt. Express* **19**(15), 14188–14199 (2011).
38. A. Curatolo, J. S. Birkenfeld, E. Martinez-Enriquez, J. A. Germann, G. Muralidharan, J. Palaci, D. Pascual, A. Eliasy, A. Abass, J. Solariski, K. Karnowski, M. Wojtkowski, A. Elsheikh, and S. Marcos, "Multi-meridian corneal imaging of air-puff induced deformation for improved detection of biomechanical abnormalities," *Biomed. Opt. Express* **11**(11), 6337–6355 (2020).
39. D. Bronte-Ciriza, J. S. Birkenfeld, A. de la Hoz, A. Curatolo, J. A. Germann, L. Villegas, A. Varea, E. Martinez-Enriquez, and S. Marcos, "Estimation of scleral mechanical properties from air-puff optical coherence tomography," *Biomed. Opt. Express* **12**(10), 6341–6359 (2021).
40. N. Bekesi, C. Dorransoro, A. de la Hoz, and S. Marcos, "Material properties from air puff corneal deformation by numerical simulations on model corneas," *PLoS One* **11**(10), e0165669 (2016).
41. B. A. Nguyen, C. J. Roberts, and M. A. Reilly, "Biomechanical Impact of the Sclera on Corneal Deformation Response to an Air-Puff: A Finite-Element Study," *Front. Bioeng. Biotechnol.* **6**, 210 (2019).
42. F. Zvietovich, A. Nair, M. Singh, S. R. Aglyamov, M. D. Twa, and K. V. Larin, "Dynamic Optical Coherence Elastography of the Anterior Eye: Understanding the Biomechanics of the Limbus," *Invest. Ophthalmol. Vis. Sci.* **61**(13), 7 (2020).
43. A. Ramier, A. M. Eltony, Y. Chen, F. Clouser, J. S. Birkenfeld, A. Watts, and S. H. Yun, "In vivo measurement of shear modulus of the human cornea using optical coherence elastography," *Sci. Rep.* **10**(1), 17366 (2020).

44. A. Ramier, B. Tavakol, and S. H. Yun, "Measuring mechanical wave speed, dispersion, and viscoelastic modulus of the cornea using optical coherence elastography," *Opt. Express* **27**(12), 16635–16649 (2019).
45. A. Ramier, J. T. Cheng, M. E. Ravicz, J. J. Rosowski, and S. H. Yun, "Mapping the phase and amplitude of ossicular chain motion using sound-synchronous optical coherence vibrography," *Biomed. Opt. Express* **9**(11), 5489–5502 (2018).
46. N. Bekesi, P. Gallego-Munoz, L. Ibares-Frias, P. Perez-Merino, M. C. Martinez-Garcia, I. E. Kochevar, and S. Marcos, "Biomechanical changes after in vivo collagen cross-linking with rose bengal-green light and riboflavin-UVA," *Invest. Ophthalmol. Vis. Sci.* **58**(3), 1612–1620 (2017).
47. B. A. Gawargious, A. Le, M. Lesgart, S. Ugradar, and J. L. Demer, "Differential regional stiffening of sclera by collagen cross-linking," *Curr. Eye Res.* **45**(6), 718–725 (2020).
48. Glaukos, "Glaukos. Transforming vision," (2022), retrieved 01/13/2022, 2022, <https://www.glaukos.com/int/cornea/kxl-system/>.
49. G. Y. Li, Y. Zheng, Y. X. Jiang, Z. Zhang, and Y. Cao, "Guided wave elastography of layered soft tissues," *Acta Biomater.* **84**, 293–304 (2019).
50. Z. Han, J. Li, M. Singh, C. Wu, C. H. Liu, R. Raghunathan, S. R. Aglyamov, S. Vantipalli, M. D. Twa, and K. V. Larin, "Optical coherence elastography assessment of corneal viscoelasticity with a modified Rayleigh-Lamb wave model," *J. Mech. Behav. Biomed. Mater.* **66**, 87–94 (2017).
51. A. Nair, C. Wu, M. Singh, C. H. Liu, R. Raghunathan, J. Nguyen, M. Goh, S. Aglyamov, and K. Larin, *Evaluation of posterior porcine sclera elasticity in situ as a function of IOP* SPIE BiOS (SPIE, 2018), Vol. 10474.
52. M. Singh, A. Nair, S. Aglyamov, C. Wu, Z. Han, E. Lafon, and K. Larin, *Assessing the changes in the spatial stiffness of the posterior sclera as a function of IOP with air-pulse OCE*, SPIE BiOS (SPIE, 2017), Vol. 10067.
53. L. Villegas, J. Germann, and S. Marcos, "Biomechanical effects of Scleral crosslinking using Rose Bengal/Green-light and Rivoflavin/UVA," *Invest. Ophthalmol. Vis. Sci.* **62**(8), 2281 (2021).
54. J. Germann, L. Villegas, E. Martinez-Enriquez, L. Revuelta, B. C  mitre, D. Sanderson, V. Llorente, M. Desco, M. V. G  mez-Gaviro, and S. Marcos, "Collagen Organization in the Posterior Rabbit Sclera Post Cross-Linking," *Invest. Ophthalmol. Vis. Sci.* **62**, 3276 (2021).
55. J. K. Pijanka, P. P. Markov, D. Midgett, N. G. Paterson, N. White, E. J. Blain, T. D. Nguyen, H. A. Quigley, and C. Boote, "Quantification of collagen fiber structure using second harmonic generation imaging and two-dimensional discrete Fourier transform analysis: Application to the human optic nerve head," *J. Biophotonics* **12**(5), e201800376 (2019).
56. G. Y. Li and Y. Cao, "Assessing the mechanical properties of anisotropic soft tissues using guided wave elastography: Inverse method and numerical experiments," *J. Acoust. Soc. Am.* **142**(3), 1526–1536 (2017).
57. J. J. Pitre Jr., M. A. Kirby, D. S. Li, T. T. Shen, R. K. Wang, M. O'Donnell, and I. Pelivanov, "Nearly-incompressible transverse isotropy (NITI) of cornea elasticity: model and experiments with acoustic micro-tapping OCE," *Sci. Rep.* **10**(1), 12983 (2020).
58. J. C. Downs, J. K. Suh, K. A. Thomas, A. J. Bellezza, R. T. Hart, and C. F. Burgoyne, "Viscoelastic material properties of the peripapillary sclera in normal and early-glaucoma monkey eyes," *Invest. Ophthalmol. Visual Sci.* **46**(2), 540–546 (2005).
59. M. Chiquet, M. Matthisson, M. Koch, M. Tannheimer, and R. Chiquet-Ehrismann, "Regulation of extracellular matrix synthesis by mechanical stress," *Biochem. Cell Biol.* **74**(6), 737–744 (1996).
60. S. J. J. Kwok, M. Kim, H. H. Lin, T. G. Seiler, E. Beck, P. Shao, I. E. Kochevar, T. Seiler, and S. H. Yun, "Flexible optical waveguides for uniform periscleral cross-linking," *Invest. Ophthalmol. Visual Sci.* **58**(5), 2596–2602 (2017).